Proceedings of ASME Turbo Expo 2010: Power for Land, Sea and Air
GT2010
June 14-18, 2010, Glasgow, UK

GT2010-22006

THE PERFORMANCE OF A GENERIC NON-AXISYMMETRIC END WALL IN A SINGLE STAGE, ROTATING TURBINE AT ON AND OFF-DESIGN CONDITIONS

Glen Snedden and Dwain Dunn
CSIR
Pretoria, South Africa

Grant Ingram and David Gregory-Smith
Durham University
Durham, United Kingdom

ABSTRACT

The application of non-axisymmetric end walls in turbine stages has gained wide spread acceptance as a means to improve the performance of turbines in both power generation and aero-derivative applications. Non-axisymmetric end walls are aimed at the control of secondary flows and to a large extent have been developed through the use of computational fluid dynamics and detailed measurements in linear and annular cascades and proven in full scale engine tests. Little or no literature is available describing their performance at conditions other than design.

This study utilises 5-hole probe measurements in a low speed, model turbine in conjunction with computational fluid dynamics to gain a more detailed understanding of the influence of a generic end wall design on the structure of secondary flows at both on and off-design flow conditions.

Results indicate a 0.4% improvement in rotor efficiency at design but this was reduced at off design and at higher loading the rotor efficiency was reduced by 0.5%. Stage efficiencies were improved for all conditions but with a declining trend as load was increased. Experimental and CFD results are examined to investigate these findings further.

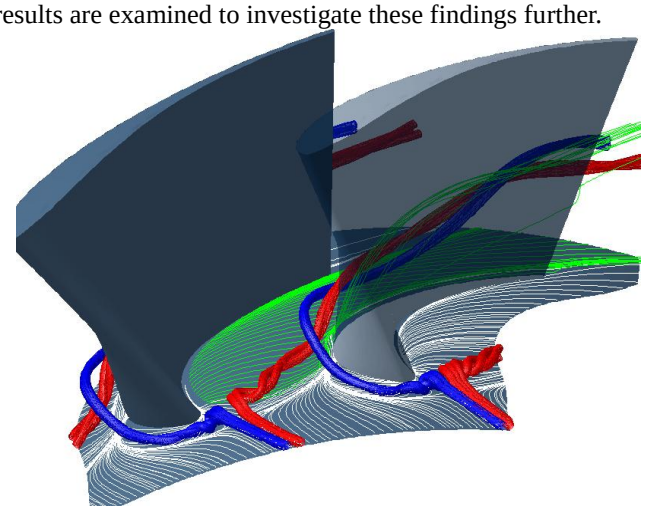

Figure 1: Turbine secondary flows

NOMENCLATURE

α	Absolute Flow Angle
β	Relative Flow Angle
η_{tt}	Total-Total Efficiency
CFD	Computational Fluid Dynamics
C_{ske}	Coefficient of Secondary Kinetic Energy
C_x	Axial Velocity
h	Enthalpy
HP	High Pressure
IP	Intermediate Pressure
LP	Low Pressure
NGV	Nozzle Guide Vane
P	Pressure
SST	Shear Stress Transport
T	Temperature
U	Wheel Speed (m/s)
V	Absolute Velocity (m/s)
w	Specific work
W	Relative Flow Velocity (m/s)
X0, X1, X2, X3, X4	Traverse positions (see Fig. 2)

Subscripts:

0	Stagnation
2	Rotor entrance
3	Rotor exit
is	isentropic
m	Mean
r	Radial
sec	Secondary flow component

INTRODUCTION

Non-axisymmetric or profiled end walls have been successfully applied to a number of test and in service turbines such as the high and intermediate pressure stages of the Trent 500 [1, 2, 3] and the Trent 900 [4]. The purpose of these end walls is to control or mitigate secondary flows generated when the incoming flow, which includes an end wall boundary layer, is deflected through the blade passage.

End wall secondary flows may be responsible for as much as a third of the losses found in a turbine row depending on factors such as aspect ratio and tip clearance [5], and hence the emphasis on the alleviation of these undesirable flow features. While the detailed descriptions of secondary flows are best left to the other authors in the field [6, 7, 8] the one common misconception is the number of rotations of the vortical structure depicted schematically by many authors. In the accelerating flows associated with turbines the energy addition resulting from this acceleration serves to stretch the vortices resulting in only a few rotations as they pass through the turbine passage as is depicted in Fig. 1.

In Fig. 1, coloured stream tubes are used to indicate the suction side leg of the horseshoe vortex (blue) which remains close to the suction surface, held there by the pressure gradient, and the pressure side leg of the horseshoe vortex (red). The pressure side leg of horseshoe vortex is driven across the passage by the pressure gradient in the same direction as the end wall cross flow (green streamlines). The pressure side leg of the horseshoe vortex is then observed to collide and combine with or wrap around the suction side leg of the horseshoe vortex and together climb the suction surface and grow in physical size with the further combination of the passage cross flow. The passage vortex results from low momentum flow on the blade and end wall boundary layer being driven across the passage by the pressure difference between pressure and suction surfaces of adjacent blades.

Further pairs of vortices have been observed at the blade root corners, emanating from behind the saddle point. These are known as corner vortices [8].

In the absence of transonic flow the basic profiled end wall design is aimed at reducing the end wall cross flow by affecting the pressure gradient. The design consists of a "hill" which reduces the local passage area in an attempt to increase the flow speed and hence decrease the pressure against the pressure surface of the blade, and a "valley" strategically placed close to the suction surface reduces the velocity, increasing the local pressure. Another way to look at this is that the blades become effectively aft loaded in the vicinity of the contoured end walls. The latter description is what best describes the thrust of research presented by various authors from Carleton University and Pratt and Whitney [9-14] who, using cascade tests and CFD, have studied a series of increasingly more highly loaded blade profiles together with end wall contouring. This has been in an effort to exploit the inherently low mid-span loss of forward loaded blades profiles in low pressure turbines while exploiting non-axisymmetric end wall technology on the hubs to mitigate the associated increased secondary flows resulting from forward loading. In 2007 Zoric *et al.* [11] presented results for the relatively lightly loaded PAK-B cascade as well as the highly loaded aft and forward loaded PAK-D designs at three incidences. The conclusions from this work noted the increasing strength of the passage vortex with increased loading and the good performance of the forward loaded PAK-D cascade across the incidence range while the aft loaded design stalled at positive incidence. This work, however, did not include the effect of profiled end walls at off design incidence.

This leaves the only two studies available to the author that examine the use of profiled end walls at off-design incidence to be the model Trent engine rig tests presented by Rose *et al.* [2] and Harvey *et al.* [3]. These authors found conflicting trends for their HP and IP designs however. Despite using the same end wall optimisation approach and achieving the expected stage efficiency improvements at design, the HP turbine stage efficiency results showed the profiling to have the greatest effect at the highest loading and virtually no effect at the lightly loaded case, while the complete opposite is true of the IP turbine. In both cases the end wall profiling was observed to restrict the secondary losses to closer to the end wall and therefore to deteriorate the total pressure profile at exit to the turbine but without significantly impacting on the efficiency of the downstream row. Furthermore they noted in the latter paper [3] that it might be interesting to use an off-design component during optimization, something that seems more broadly accepted in the compressor community where profiled end walls are being investigated of late and have been shown to delay the effects of corner stall [15].

The purpose of this study is to compare the use of a profiled end wall design [16] with that of an annular end wall in a 1½ stage rotating test rig at both on and off-design conditions. Five-hole steady state probe measurements are presented with CFD being used to provide detailed information of the flow in the passage.

EXPERIMENTAL SETUP

Figure 2 indicates the general layout and instrumentation of the 1½ stage test rig used for this work, and a more complete description of both the test rig and methodology as well as the blading can be found in [16, 17]. In summary, the rotor blades were designed to have the Durham cascade profile at the rotor hub in order to utilise an end wall profile similar to one used in the Durham cascade. Figure 3 shows a picture of the completed blade.

The rotor tip gap is relatively large at 1.7% of span, while that for the stators is 0.8% of span. Fillet radii of 1mm are used at the junction between blade and end wall.

The hub Reynolds number based on axial chord at rotor exit is approximately 127 500 compared to the Durham cascade at 400 000.

Blade numbers were selected to ensure direct comparison to CFD without geometrical scaling for later unsteady CFD analysis, and to restrict axial chord length to that available in the test rig. The resulting blade numbers were 30 stators and 20 rotor blades.

The test rig allows for independent control of the rotor wheel speed and the inlet mass flow or axial velocity. For the purposes of these tests the inlet axial velocity was held constant at 21.38m/s, while the wheel speed was set to 1907, 2300 or 2820 RPM to give approximately +5° incidence in the highly loaded case, 0° at design, and -5° incidence in the reduced loading case at the hub, respectively, see Fig. 4. The flow coefficient is controlled to a constant set-point throughout a given traverse.

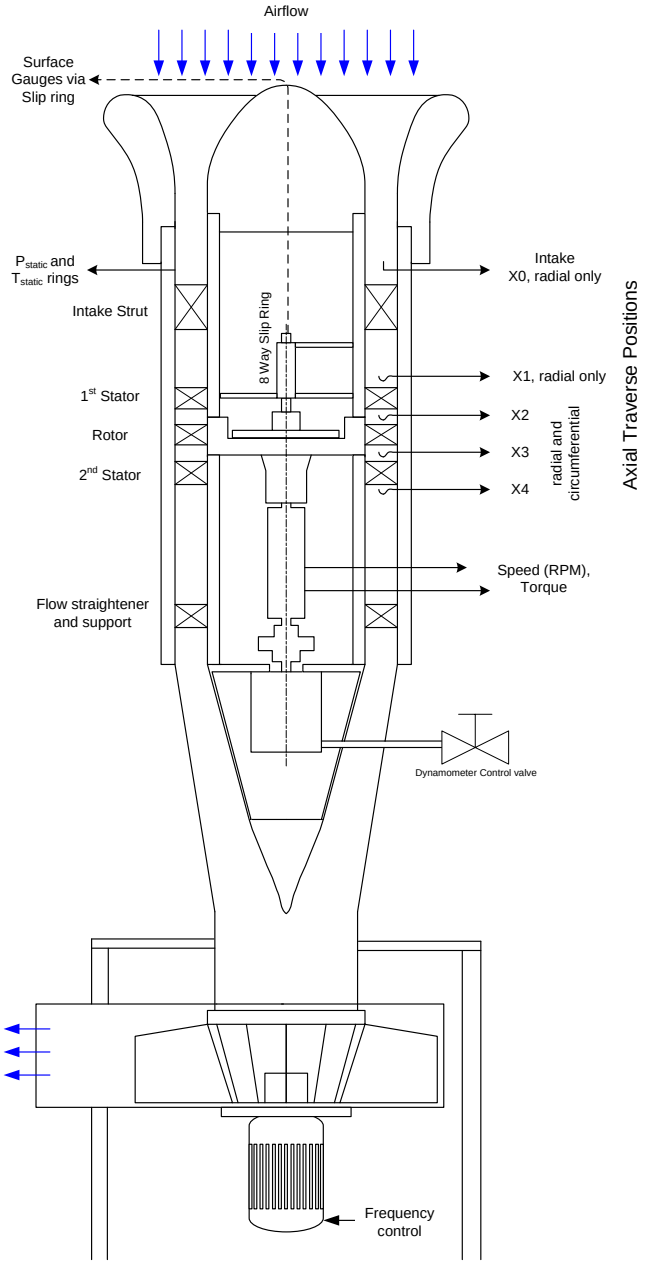

Figure 2: Schematic of 1½ stage turbine showing control and measurement instrumentation

Inlet turbulence intensity was measured to be less than 1%. 5-Hole probe measurements followed the methodology of Ingram and Gregory-Smith [18].

Experimental uncertainty on stage efficiency has been determined stochastically [24], using an experimental dataset as the basis, to be less than ±0.2% (as indicated in Fig. 6) using the transducers described in Table 1. Should all the uncertainties work together in a worst case scenario then this result approaches ±0.6%. Three replications of results between complete rebuilds of the test rig have shown efficiency to repeat to a level of less than ±0.45% while C_{ske} does so to less than ±0.4% (as indicated in Fig. 6).

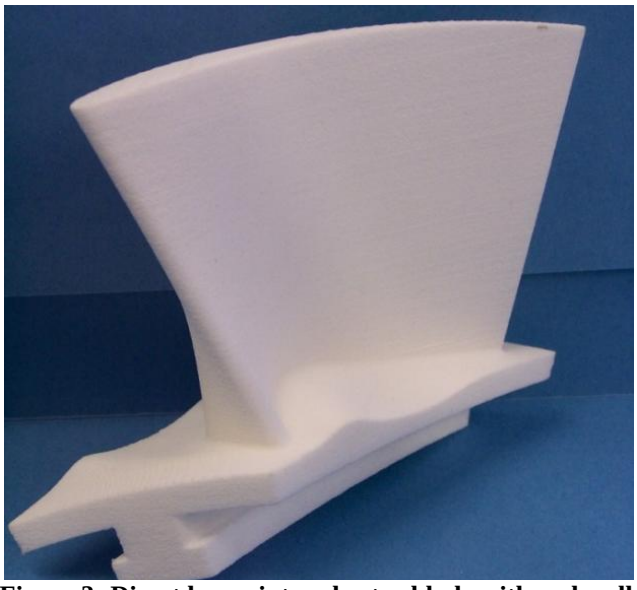

Figure 3: Direct laser sintered rotor blade with end wall contouring

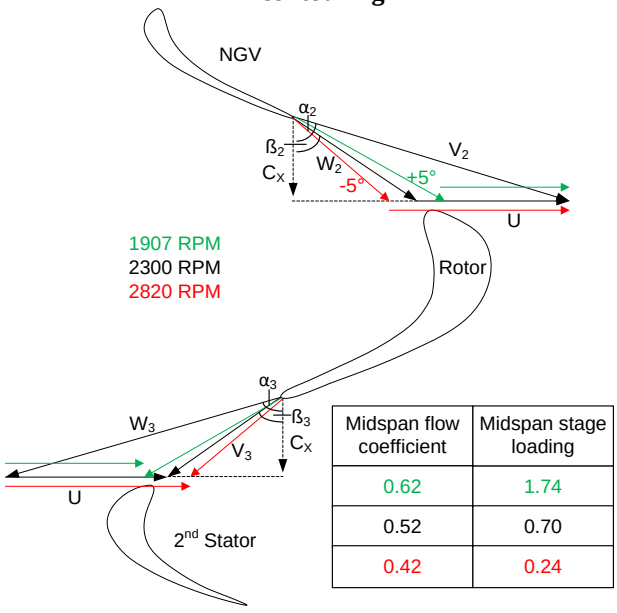

Midspan flow coefficient	Midspan stage loading
0.62	1.74
0.52	0.70
0.42	0.24

Figure 4: Flow triangles for on- and off-design operation

Table 1: Primary instrumentation

Parameter	Instrument	Uncertainty
Torque	Himmelstein MCRT 28002T(5-2)CNA-G + Model 721	±0.03N.m
Speed		2RPM
Barometric Pressure	Siemens Sitrans P 7MF4233-1FA10-1AB6-Z A02+B11	0.075% of full scale
Differential Pressure	5 x Siemens Sitrans P 7MF4433-1CA02-1AB6-Z A02+B11	0.075% of full scale
Temperature	PT1000 RTD's	±0.05°C

COMPUTATIONAL FLUID DYNAMICS

As with the previous study [16] the CFD code chosen for this work was Numeca Fine™/TURBO v8 [19] and the mesh is unchanged, see Fig. 5. Three stator passages and two rotor passages were modelled as part of the steady state solutions where a mixing plane with conservative coupling is located at the stator/rotor and rotor/stator interfaces.

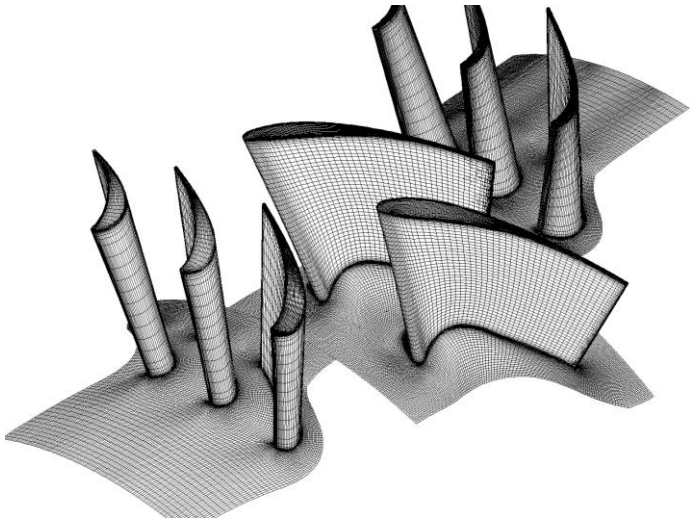

Figure 5: CFD mesh

Both the Baldwin-Lomax and SST k-ω models were used throughout this study as per Dunn *et al.* [20]. Both turbulence models are implemented as standard in Fine™/TURBO v8, without custom coefficients.

The fillets between the blade and end wall are not modelled. This is contrary to the recommendations of Germain *et al.* [21], a study that indicated the importance of modeling the fillets, but which emerged after completion of the CFD mesh for this case.

RESULTS

No comparison of the nozzle outlet flows are included in this analysis as the axial velocity is held constant resulting in flows that are essentially unchanged from those reported in [16].

Figure 6 compares three of the most common measures of stage and rotor performance relevant to this case. The Coefficient of Secondary Kinetic Energy (C_{ske}) is adapted from Ingram [23]:

$$C_{ske} = \frac{V_{sec}^2 + V_r^2}{C_x^2}$$

where:

$$V_{sec} = V \cdot \sin(\alpha - \alpha_m)$$

This coefficient has proven to be an effective proxy for secondary kinetic energy and is extensively published as an objective function for end wall optimization [1, 25, 26].

Efficiency has been calculated using torque measured and computed and data extracted at identical points to those of the experiment. Making isentropic and incompressible assumptions for the low speed turbine means that the turbine total efficiency can be expressed as:

$$\eta_{tt} = \frac{w}{h_{01} - h_{03}} = \frac{w}{(h_{01} - h_{3is}) - \frac{1}{2}V_{3is}^2} = \frac{w}{\frac{P_{01} - P_{3is}}{\rho} - \frac{1}{2}V_{3is}^2}$$

Similar expressions are possible for rotor efficiency by replacing P_{01} with P_{02}.

The most obvious differences between experiment and CFD results for all the mass averaged quantities examined is the large disparities between the efficiency levels reported. In the case of efficiency the level differences cannot be attributed to windage and bearing loss, and these quantities have been ignored as their effect is small (<0.05% of turbine power). Generally speaking the CFD results over-predict efficiency. Absolute values of efficiency are absent from the literature, leaving the authors unsure if such a large discrepancy is common or not. Overall the experiments predicted a small increase in efficiency with decreasing load, while the trends of secondary kinetic energy show a larger reduction in secondary kinetic energy at higher loading when secondary flows are expected to be more severe and a reversal in trend at low loads. SST k-ω CFD results show an increasing improvement with increasing load and the implementation of end walls, but no reversal, only convergence at light loads. The Baldwin-Lomax C_{ske} trends produce an unexpected result for the higher load case, possible as a result of the simplified turbulence models' inability to transport viscous information through the domain effecting the generation of vorticity. Only stage efficiency experimental results show a clear across the board improvement with the implementation of profiled end walls.

If one restricts the analysis to just the differences between end wall options for a given parameter, the CFD and experiment fall much closer together, however the loading trends are erratic, but it should also be noted that most of these differences are small and close to the experimental replication band.

Figures 7 to 10 examine some of these parameters as well as the more fundamental quantities of rotor outlet flow angle and velocity as span-wise distributions in an attempt to make more sense of the results.

In Fig. 7 the effect of increased incidence is apparent in the development of an over speed region in the 0 to 30% span location which increases in speed and span-wise extent with increased load. This is balanced by a decrease in the relative velocities in the tip region which likewise expands in depth and span-wise extent. The introduction of profiled end walls reduces the extent of the hub secondary flow region very slightly in the experimental results at design. The same is quite clearly demonstrated in the SST k-ω CFD case in all cases but is only really evident in the high load case using the Baldwin-Lomax model. However the opposite is true at 1907 RPM in the experimental case. The inset contour plots serve to illustrate the CFD trends even more clearly. Profiled end walls consistently, in both the experimental and CFD analysis detrimentally effect the tip leakage flows, something that is again well illustrated by the contour plots.

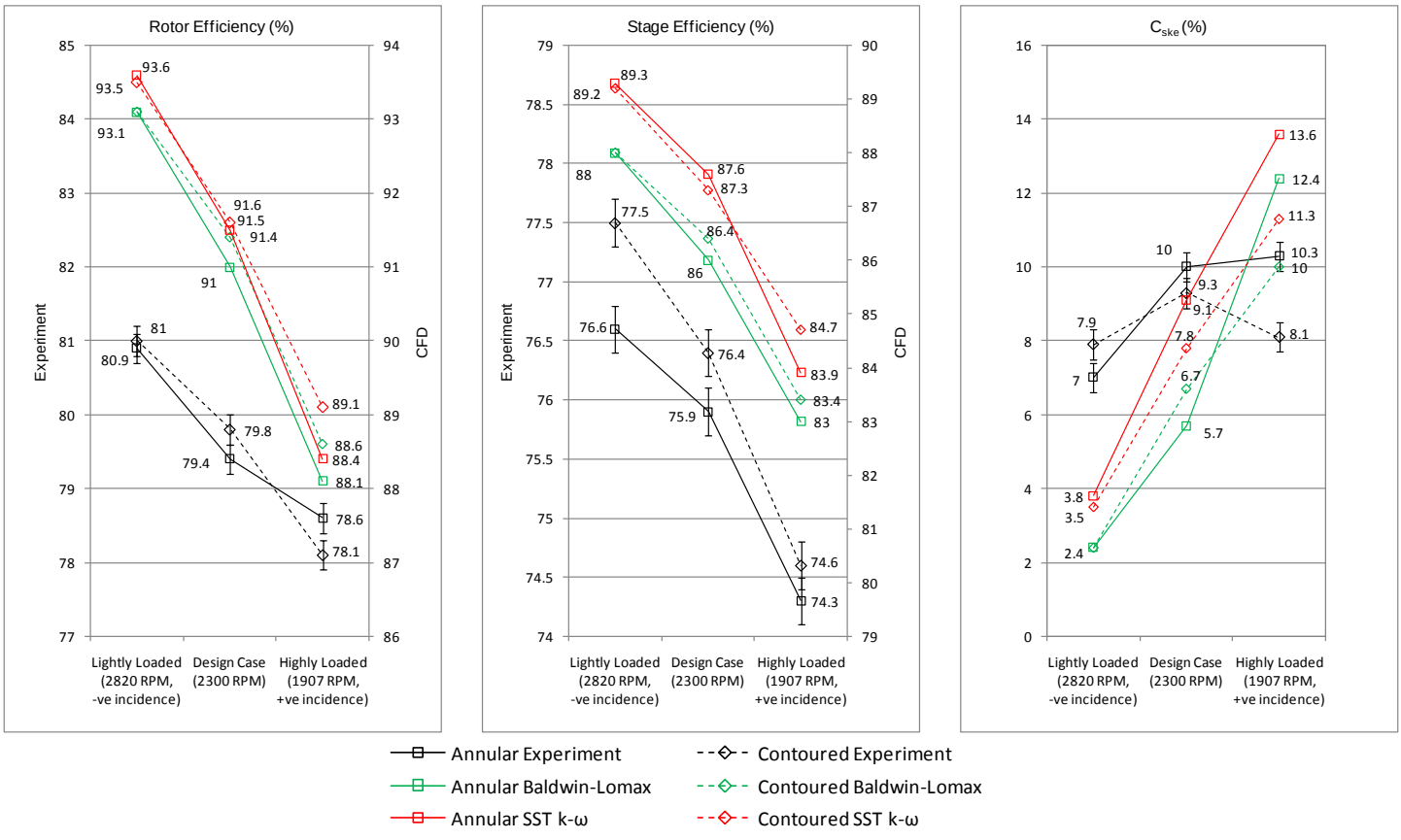

Figure 6: Rotor, Stage Efficiency and Coefficient of Secondary Kinetic Energy Comparisons

Figure 8 shows the rotor relative outlet flow angle, and here one can note a consistent improvement as a result of the introduction of profiled end walls, particularly from the SST k-ω and experimental results. This is the suppression of the overturning at the hub towards the hub, this is particularly true in the 10 to 20% span region, however as was found by both [2] and [3] this is balanced by an increase in the magnitude of the overturning angle. In addition the profiling generally reduces the exit flow angle variability. At the tip the trend with regard to increasing load is to reduce the deviation from the design flow angles experimentally, however and more intuitively the CFD predicts an increase in tip leakage flows. The inset contour plots again illustrate these effects nicely, clearly indicating a softening of the secondary flow effects in the bulk flow region with the introduction of profiled end walls and the deepening of the region of overturned flow at the hub.

Figure 9 plots span-wise results for C_{ske} and a clear pattern emerges with the suppression of secondary kinetic energy both at mid-span and at the hub with the introduction of profiled end walls. Secondary energy levels increase with loading as turning increases and are very low at the highest speed and as a result little difference can be seen with or without profiling. At design and high load the differences are clear and the mid-span secondary kinetic energy is reduced and the hub features suppressed toward the end wall. SST k-ω tends to over predict the extent of the span-wise feature but does capture the features close to the hub well with the profiled endwalls implemented.

In an attempt to visualize the three dimensional features of the flow, Fig. 10 shows red and blue stream tubes representing the pressure and suction side legs of the horseshoe vortex respectively while the grey ribs allow one to visualize the tip leakage flows and the purple ribbons the cross passage flows at the hub. The contours of exit relative flow angle aid in understanding the condition of the flow at exit. In all cases the profiled end walls results in a high degree of over-turning at the hub, which can be seen to result from the modification of the passage cross flow angle which results in over-turned flow passing behind the trailing edge rather than colliding with the blade and becoming caught in the combined passage vortices. The exit flow angle also tends to be qualitatively more uniform with the introduction of end walls, with the high turning area at roughly 30% span being reduced in influence. For the annular case the passage vortices combine with the suction leg wrapping around the pressure leg, both legs making slightly less than one turn down the length of the passage. As load increases the annular case indicates an increase in the span-wise movement of the combined vortex system as the turning increases. The same span-wise movement is seen in the pressure side leg of the horseshoe vortex in the profiled end wall case, however the suction side leg is increasingly remote from the pressure side leg as load increases, to the extent that the suction side leg is unattached and emerges at roughly 25% span at the highest load. The tip leakage flows in Fig. 10 are of great interest, as they descend span-wise to the extent that they interact with hub secondary flow features as is borne out by the experimental evidence of the influence of the end wall contouring on the tip leakage flows. At the lowest load condition the tip leakage flows are only slightly affected by the

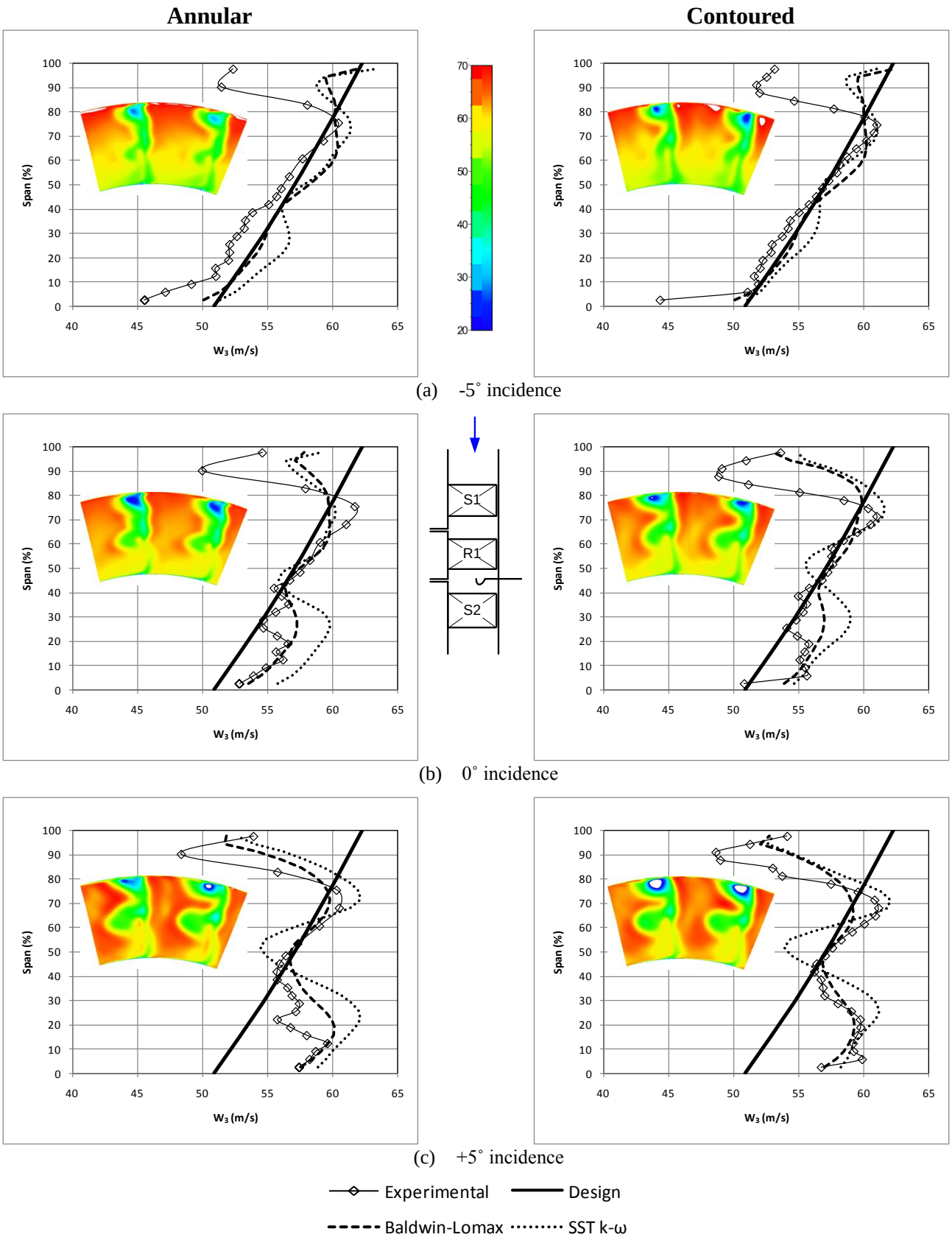

Figure 7: Pitch averaged relative rotor outlet velocity (SST k-ω CFD area plot inset)

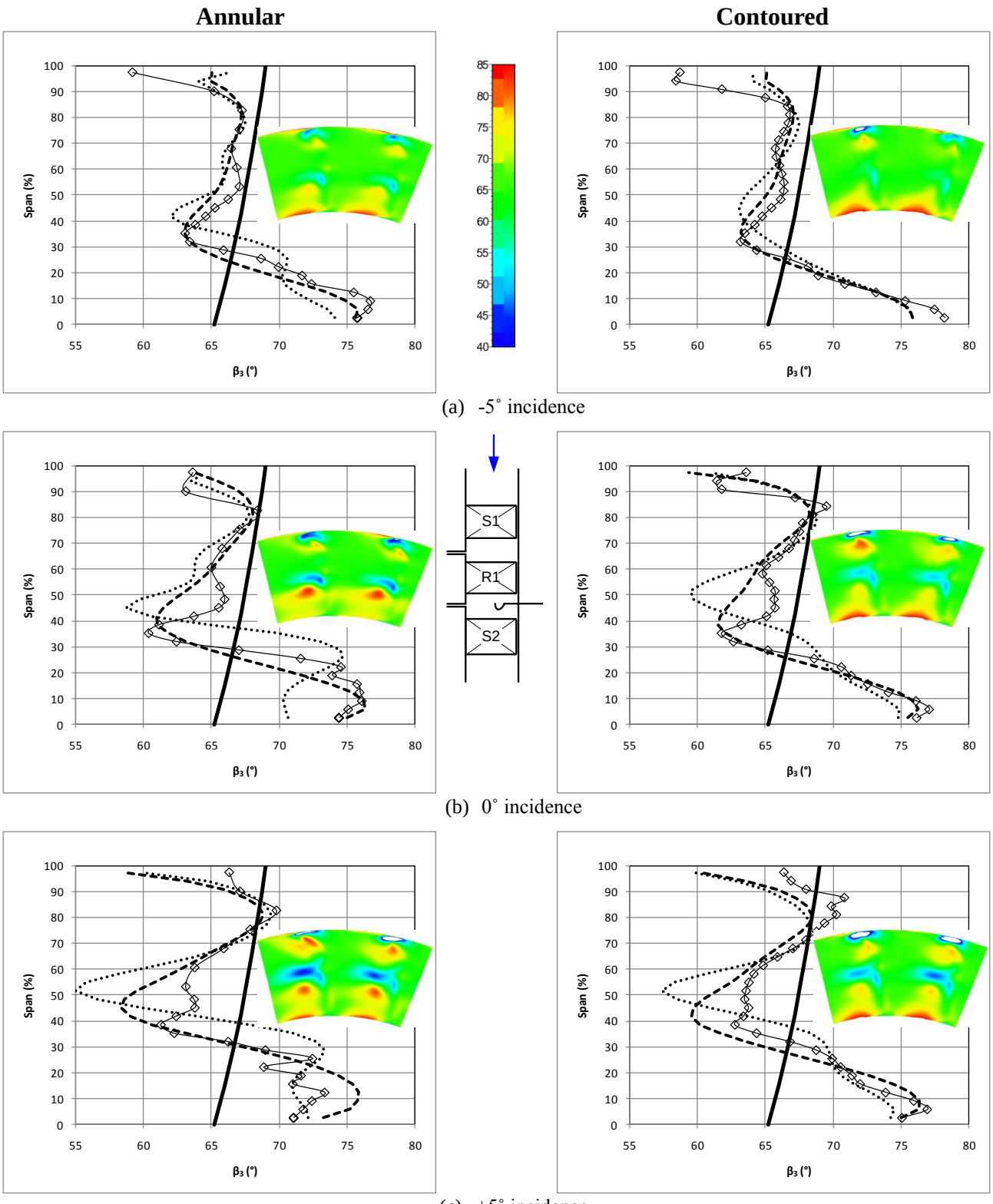

Figure 8: Pitch averaged relative rotor outlet angle (SST k-ω CFD area plot inset)

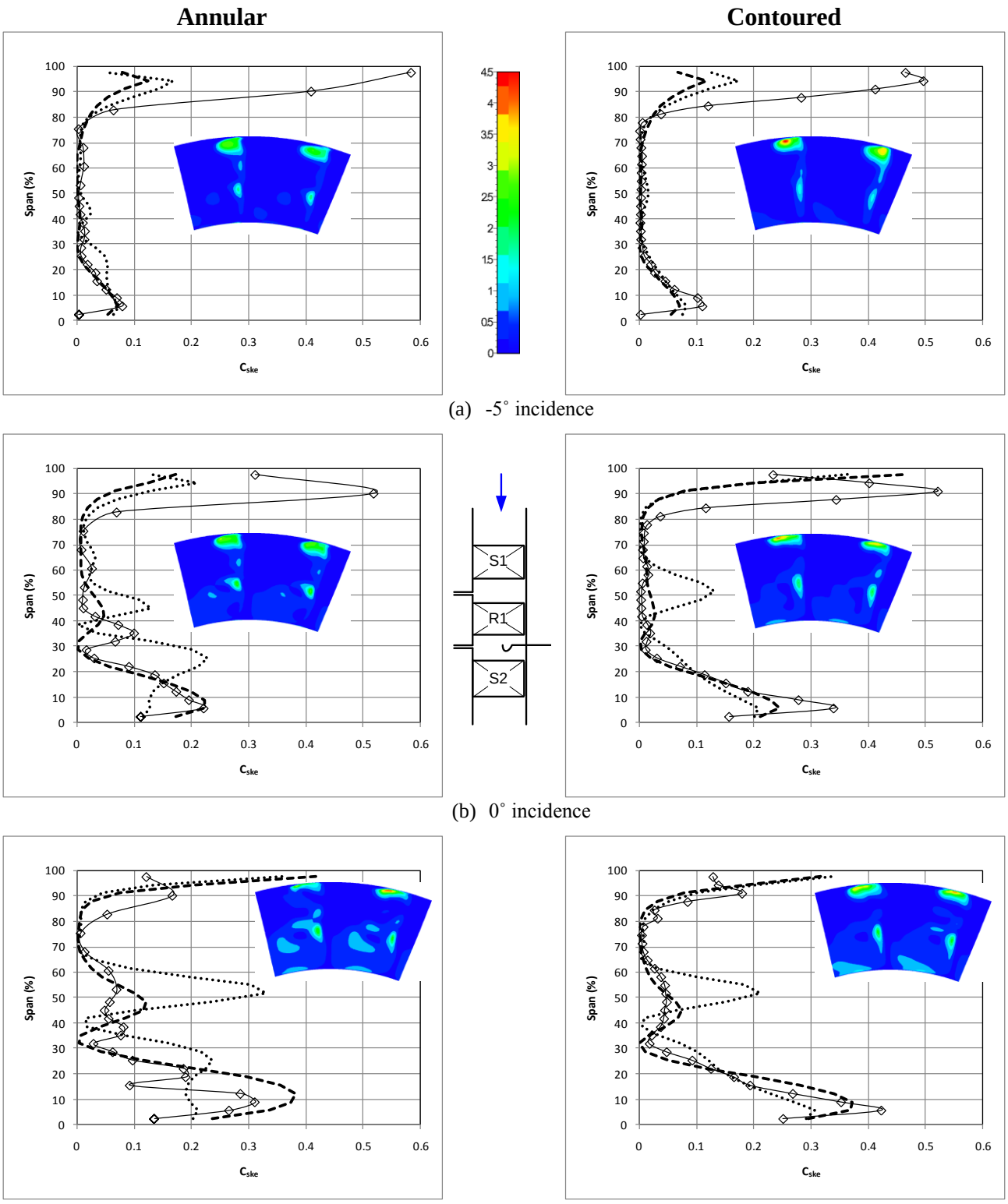

Figure 9: Rotor outlet coefficient of secondary kinetic energy (SST k-ω CFD area plot inset)

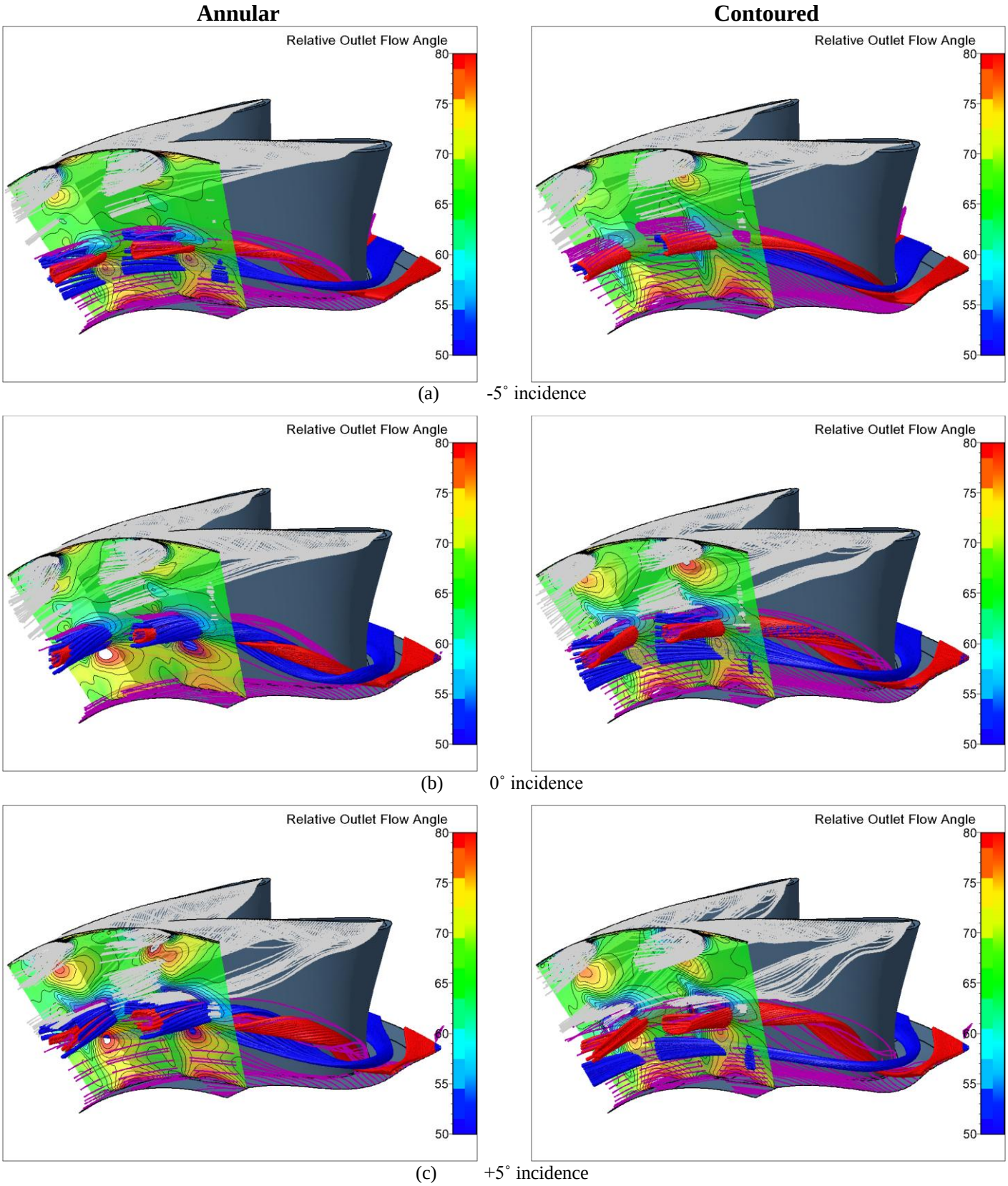

Figure 10: SST k-ω CFD, Contoured rotor: Relative outlet flow angle and vortex stream tubes

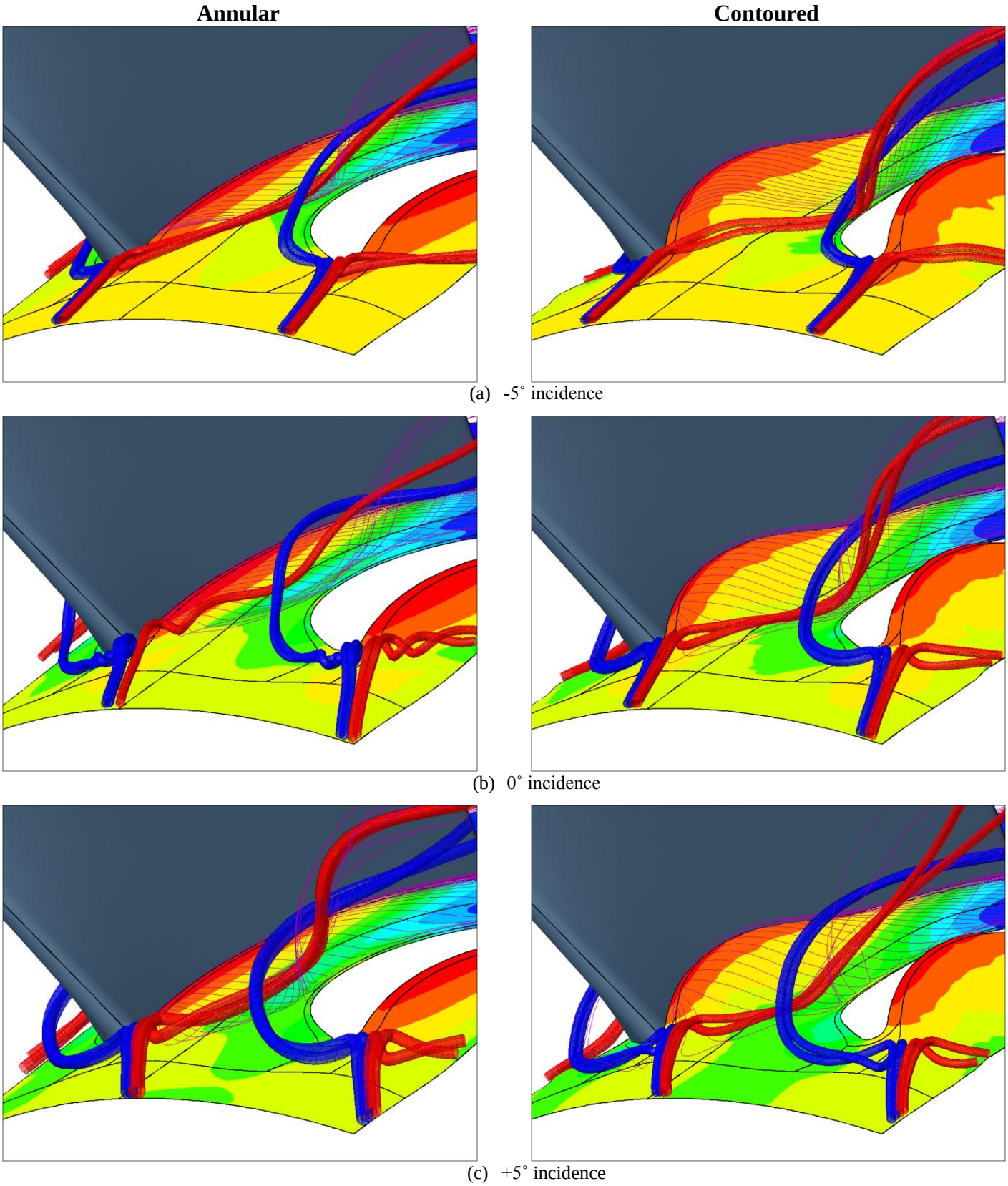

Figure 11: SST k-ω CFD, Contoured rotor: Close up of passage vortex streamlines (Pressure contours are plotted on the hub to indicate the driving gradients, the colour range is different for each figure)

introduction of profiled end walls. At the design condition, however, the tip leakage flow has separated into two or three distinct regions – a fore and aft feature separated possibly by the unloading at mid-chord. At the highest load condition both annular and profiled end walls exhibit this same influence on the tip leakage separating into two distinct vortices, but in the profiled end wall case its span wise descent is more rapid.

In an attempt to visualize the three dimensional features of the flow, Fig. 10 shows red and blue stream tubes representing the pressure and suction side legs of the horseshoe vortex respectively while the grey ribs allow one to visualize the tip leakage flows and the purple ribbons the cross passage flows at the hub. The contours of exit relative flow angle aid in understanding the condition of the flow at exit. In all cases the profiled end walls results in a high degree of over-turning at the hub, which can be seen to result from the modification of the passage cross flow angle which results in over-turned flow passing behind the trailing edge rather than colliding with the blade and becoming caught in the combined passage vortices. The exit flow angle also tends to be qualitatively more uniform with the introduction of end walls, with the high turning area at roughly 30% span being reduced in influence. For the annular case the passage vortices combine with the suction leg wrapping around the pressure leg, both legs making slightly less than one turn down the length of the passage. As load increases the annular case indicates an increase in the span-wise movement of the combined vortex system as the turning increases. The same span-wise movement is seen in the pressure side leg of the horseshoe vortex in the profiled end wall case, however the suction side leg is increasingly remote from the pressure side leg as load increases, to the extent that the suction side leg is unattached and emerges at roughly 25% span at the highest load. The tip leakage flows in Fig. 10 are of great interest, as they descend span-wise to the extent that they interact with hub secondary flow features as is borne out by the experimental evidence of the influence of the end wall contouring on the tip leakage flows. At the lowest load condition the tip leakage flows are only slightly affected by the introduction of profiled end walls. At the design condition, however, the tip leakage flow has separated into two or three distinct regions – a fore and aft feature separated possibly by the unloading at mid-chord. At the highest load condition both annular and profiled end walls exhibit this same influence on the tip leakage separating into two distinct vortices, but in the profiled end wall case its span wise descent is more rapid.

Finally Fig. 11 examines the early development of the horseshoe vortices and cross passage flow for each case. In the annular case, the red stream tube of the pressure side leg of the horseshoe vortex clearly crosses the passage with increasing helicity and at a more tangential angle with increasing load, the latter also being true for the cross passage flows marked with purple streamlines. Because of this increased tangential component the impact of the pressure side leg of the vortex on the suction side of the blade is much steeper. The profiled end walls on the other hand show little difference in the angle of the passage crossing of the pressure side leg of the horseshoe vortex as load increases, although angle at which it crosses the passage is more tangential than any of the annular cases making its rise up the suction surface of the blade very steep. The cross-passage flow does become more tangential in the mid to aft section of the passage as load increases but is less tangential than the equivalent annular case. In the early part of the passage however the profiling results in upstream movement of the cross-passage flow and at high load some even escapes around the leading edge to the suction surface.

CONCLUSIONS

The application of a generic profiled end wall to a turbine rotor blade has been examined in detail across a range of loads using both a rotating experiment and CFD. As expected, increased load and effectively turning increases the magnitude and span-wise extent of the hub secondary flows as is evidenced by plots of relative flow velocity and angle as well as coefficient of secondary kinetic energy at exit to the rotor. The end wall has a strong influence on the secondary flows, most notably to:

- Fix the angle at which the pressure side leg of the horseshoe vortex crosses the passage
- Reduce the tangential velocity component of the cross passage flow in the mid to aft portion of the passage crosses which results in a reduction in the strength of the passage vortex, but instead results in a high degree of overturning close to the hub as reported by other authors [2,3] who also assert that this has little effect on downstream rows as a result of its limited span-wise influence.

In addition the generic contour yields two unintended consequences:

- Upstream movement of flow in the boundary layer ahead of the raised portion of the profile
- Contouring has an effect on the tip leakage flow. The exact mechanism of which is not yet understood.

Both of these features might potentially be eliminated through custom optimization, but at very least the effect on the tip clearance flows points towards the need for greater care in the design of end wall for free tip blading, even at these relatively high aspect ratios.

Small overall efficiency improvements (0.4% at design), of similar magnitude to those found by Harvey *et al.* [3], have been shown to be achievable although incidence has a clear influence on the effectiveness of the end walls which further indicates that, as in compressor research, off design considerations should be included in the optimization process [15]. The relatively small improvements are partly as a result of the use of the rotor in this study when other researchers [21] have shown the greatest contribution from end wall profiling is to be found in the stators.

The final conclusion of this work is to suggest that parameters such as efficiency – which are not well predicted in CFD and can be shown to be insensitive to secondary flows, are not ideal objective function parameters for the optimization of devices designed to reduce secondary flows. Instead this work suggests that a combination (after the method of Reising and Schiffer [15]) of parameters such as the coefficient of secondary kinetic energy which is well predicted and clearly identifies the strength and position of secondary flows and more fundamental parameters such as the rotor exit flow angle and its variation.

REFERENCES

[1] Brennan G., Harvey N., Rose M. G., Fomison N. and Taylor M. D., (2001) "Improving the Efficiency of the Trent 500 HP Turbine Using Non-Axisymmetric End Walls: Part 1 Turbine Design," ASME Turbo Expo 2001-GT-0444.

[2] Rose M. G., Harvey N. W, Seaman P., Newman D. A., and McManus D., (2001) "Improving the Efficiency of the Trent 500 HP Turbine Using Non-Axisymmetric End Walls. Part II: Experimental Validation," ASME Turbo Expo 2001, ASME 2001-GT-0505.

[3] Harvey N., Brennan G., Newman D. A. and Rose M. G., (2002) "Improving Turbine Efficiency Using Non-Axisymmetric Endwalls: Validation in the Multi-Row Environment and with Low Aspect Ratio Blading," ASME Turbo Expo 2002, GT-2002-30337.

[4] Gonzalez P. and Lantero M. (2006) "Low Pressure Turbine Design for Rolls-Royce TRENT 900 Turbofan", ASME Turbo Expo, GT2006-90997.

[5] Denton J. D., (1993) "Loss Mechanisms in Turbomachines," Transactions of the ASME Journal of Turbomachinery, Vol. 115, pp. 621-650.

[6] Langston L. S., (2001) "Secondary Flows in Axial Turbines – A Review", Heat Transfer in Gas Turbine Systems, Annals of the New York Academy of Sciences, Vol. 934, May 2001, pp 11-26.

[7] Sieverding C. H., (1985) "Recent Progress in the Understanding of the Basic Aspects of Secondary Flows in Turbine Blade Passages," *Transactions of ASME, Journal of Engineering for Gas Turbines and Power*, Vol. 107, pp. 248-252.

[8] Wang H. P., Olson S. J., Goldstein R. J. and Eckert E. R. G., (1997) "Flow visualization in a linear turbine cascade of high performance turbine blades," *Transactions of the ASME Journal of Turbomachinery*, Vol. 119, pp. 1-8.

[9] Mahallati A., McAuliffe B. R., Sjolander S. A. and Praisner T. J., (2007) "Aerodynamics of a Low-Pressure Turbine Airfoil at Low Reynolds Numbers Part 1: Steady Flow Measurements", ASME Turbo Expo, GT2007-27347.

[10] Zoric T., Popovic I., Sjolander S. A., Praisner T. and Grover E., (2007) "Comparative Investigation of Three Highly Loaded LP Turbine Airfoils: Part I – Measured Profile and Secondary Losses at Design Incidence", ASME Turbo Expo GT2007-27537.

[11] Zoric T., Popovic I., Sjolander S. A., Praisner T. and Grover E., (2007) "Comparative Investigation of Three Highly Loaded LP Turbine Airfoils: Part II – Measured Profile and Secondary Losses at Off-Design Incidence", ASME Turbo Expo GT2007-27538.

[12] Praisner T. J., Allen-Bradley E., Grover E. A., Knezevici D. C. and Sjolander S. A., (2007) "Application of Non-Axisymmetric Endwall Contouring to Conventional and High-Lift Turbine Airfoils", ASME Turbo Expo GT2007-27579.

[13] Knezevici D. C., Sjolander S. A., Praisner T. J., Allen-Bradley E. and Grover E. A., (2008) "Measurements of Secondary Losses in a Turbine Cascade with the Implementation of Non-Axisymmetric Endwall Contouring", ASME Turbo Expo GT2008-51311.

[14] Knezevici D. C., Sjolander S. A., Praisner T. J., Allen-Bradley E. and Grover E. A., (2009) "Measurements of Secondary Losses in a High-Lift Front-Loaded Turbine Cascade with the Implementation of Non-Axisymmetric Endwall Contouring", ASME Turbo Expo GT2009-59677.

[15] Reising S. and Schiffer H.-P., (2009) "Non-Axisymmetric End Wall Profiling in Transonic Compressors. Part I: Improving the Static Pressure Recovery at Off-Design Conditions by Sequential Hub and Shroud End Wall Profiling", ASME Turbo Expo GT2009-59133.

[16] Snedden G., Dunn D., Ingram G. and Gregory-Smith D., (2009) "The Application of Non-Axisymmetric Endwall Contouring in a Single Stage, Rotating Turbine" ASME Turbo Expo 2009, GT2009-59169.

[17] Snedden G., Roos T., Dunn D. and Gregory-Smith D. (2007) "Characterisation of a Refurbished 1½ Stage Turbine Test Rig for Flowfield Mapping Behind Blading with Non-Axisymmetric Contoured Endwalls", ISABE 2007-1363, Beijing, China.

[18] Ingram G. and Gregory-Smith D. (2005) "An Automated Instrumentation System for Flow and Loss Measurements in a Cascade", Journal of Flow Measurement and Instrumentation.

[19] Numeca International, (2005) "User Manual FINE/Turbo v8 (including Euranus) Documentation v8a," v8a edition.

[20] Dunn D., Snedden G. and Von Backstrom T. W., (2009) "Turbulence Model Comparisons for a Low Pressure 1.5 Stage Test Turbine", ISABE 2009-1258.

[21] Germain T., Nagel M., Raab I., Schuepbach P., Abhari R. S. and Rose M. (2008) "Improving Efficiency of a High Work Turbine Using Non-Axisymmetric Endwalls Part I: Endwall Design and Performance", ASME GT2008-50469.

[22] Schuepbach P., Abhari R. S., Rose M., Germain T., Raab I., and Gier J. (2008) "Improving Efficiency of a High Work Turbine Using Non-Axisymmetric Endwalls Part II: Time Resolved Flow Physics", ASME GT2008-504670.

[23] Ingram G., (2003) "Endwall Profiling for the Reduction of Secondary Flow in Turbines", PhD Thesis, Durham University, UK.

[24] Wild P. and Hockman Y. (2007) "Stochastic Modelling for Dummies", Actuarial Society of South Africa Convention, 2007.

[25] Harvey N., Rose M. G., Shahpar S., Taylor M. D., Hartland J., and Gregory-Smith D., (2000) "Non-axisymmetric Turbine End Wall Design: Part I Three dimensional Design System", *Transactions of the ASME Journal of Turbomachinery*, Vol. 122, pp. 278-285.

[26] Hartland J., Gregory-Smith D., Harvey N., and Rose M. G., (2000) "Non-axisymmetric Turbine End Wall Design: Part II Experimental Validation", *Transactions of the ASME Journal of Turbomachinery*, Vol. 122, pp. 286-293.